Journal of Nuclear Medicine, published on May 18, 2018 as doi:10.2967/jnumed.118.210294

Development of ^{64}Cu-NOTA-Trastuzumab for HER2 targeting: radiopharmaceutical with improved pharmacokinetics for human study

Sang-Keun Woo[1*], Su Jin Jang[1*], Min-Jung Seo[1], Ju Hui Park[1], Byoung Soo Kim[1], Eun Jung Kim[1], Yong Jin Lee[1], Tae Sup Lee[1], Gwang Il An[1], In Ho Song[1], Youngho Seo[2], Kwang Il Kim[1†], Joo Hyun Kang[†]

[1]Division of RI-convergence Research, Korea Institute of Radiological and Medical Sciences, Seoul 01812, Republic of Korea
[2]Department of Radiology, University of California San Francisco School of Medicine, San Francisco, CA 94143, USA

*These authors contributed equally to this work

[†]**Correspondence to:**

Joo Hyun Kang, PhD
Division of RI-convergence Research, Korea Institute of Radiological and Medical Sciences 75, Nowon-ro, Nowon-gu, Seoul, Republic of Korea
Telephone: 82-2-970-1339
Fax: 82-2-970-1341
Email: kang2325@kirams.re.kr
Kwang Il Kim, PhD
Division of RI-convergence Research, Korea Institute of Radiological and Medical Sciences 75, Nowon-ro, Nowon-gu, Seoul, Republic of Korea
Telephone: 82-2-970-1662
Fax: 82-2-970-1341
Email: kikim@kirams.re.kr

Total word count: 4,982 words

Running title: ^{64}Cu-NOTA-trastuzumab with improved PK

Abstract

Purpose The purpose of this study was to develop ^{64}Cu-labeled trastuzumab with improved pharmacokinetics for human epidermal growth factor receptor 2.

Methods Trastuzumab was conjugated with SCN-Bn-NOTA and radiolabeled with ^{64}Cu. Serum stability and immunoreactivity of ^{64}Cu-NOTA-trastuzumab were tested. Small animal PET imaging and biodistribution study were performed in HER2-positive breast cancer xenograft model (BT-474). Internal dosimetry of experimental animals was performed using the image-based approach with the Monte Carlo N-Particle Code.

Results ^{64}Cu-NOTA-trastuzumab was prepared with high radiolabel yield and radiochemical purity (>98%) and showed high stability in serum and good immunoreactivity. Uptake of ^{64}Cu-NOTA-trastuzumab was highest at 48 h after injection determined by PET imaging and biodistribution results in BT-474 tumors. The blood radioactivity concentrations of ^{64}Cu-NOTA-trastuzumab decreased bi-exponentially with time in both mice with and without BT-474 tumor xenografts. The calculated absorbed dose of ^{64}Cu-NOTA-trastuzumab was 0.048 mGy/MBq for the heart, 0.079 for the liver and 0.047 for the spleen. ***Conclusion*** ^{64}Cu-NOTA-trastuzumab was effectively targeted to the HER2-expressing tumor *in vitro* and *in vivo*, and it exhibited relatively low absorbed dose due to short residence time. Therefore, ^{64}Cu-NOTA-trastuzumab could be applied to select the right patients/right timing for HER2 therapy, to monitor the treatment response after HER2-targeted therapy, and to detect distal or metastatic spread.

Keywords: HER2, ^{64}Cu-NOTA-trastuzumab, Absorbed dose, Patient selection, Treatment response

Introduction

Human epidermal growth factor receptor 2 (HER2), a transmembrane receptor tyrosine kinase 2, is overexpressed in gastric cancer, ovary cancer, prostate cancer, and lung cancer, as well as breast cancer. HER2 is a proven therapeutic target for breast and gastric cancer (*1*,*2*); it is highly expressed in 15–20% of breast cancers, and HER2-positive characteristics are associated with more aggressive growth, poor prognosis, greater possibility of recurrence, and decreased survival compared with HER2-negative breast cancer (*3*). Several anti-HER2 agents have been successfully developed and applied to HER2-positive breast cancer including trastuzumab and pertuzumab as antibody therapeutics and lapatinib and neratinib as HER2 tyrosine kinase inhibitors (*4*).

Trastuzumab is a humanized monoclonal antibody (mAb) that targets the extracellular portion of HER2 and is the first HER2-targeted agent approved by the United States Food and Drug Administration (FDA) for the treating both early-stage and metastatic HER2-overexpressing breast cancer (*5*). For effective treatment with HER2-targeting agents, it is important to validate HER2 expression in primary tumor and metastatic sites. Although there is routine examination of HER2 expression using immunohistochemistry (IHC) or fluorescence in situ hybridization, technical problems can arise when lesions are not easily accessible by core needle biopsy including whole body metastasis. In addition, HER2 expression can vary during the course of the disease and even among tumor lesions in the same patient. Thus, a positron emission tomography (PET) imaging probe using radio-labeled antibodies based on FDA-approved trastuzumab has been studied for the noninvasive evaluation of HER2 expression (*6*). Additionally, a molecular imaging technique with radio-labeled trastuzumab could be applied to select the right timing for HER2 therapy, to monitor the treatment response after HER2-targeted therapy, and to detect distal or metastatic spread. For this purpose, several PET or single-photon emission computed tomography (SPECT) agents with trastuzumab using ^{64}Cu, ^{124}I, ^{111}In, and ^{89}Zr were developed (*7*-*10*).

Especially, ^{64}Cu-DOTA-trastuzumab using 1,4,7,10-tetraazacyclodecane-1,4,7,10-tetraacetic acid (DOTA) as bifunctional chelator was developed and applied to clinical studies for the individualizing treatment of HER2 positive metastatic tumor as well as HER2 positive breast cancer (*11-15*).

In addition, a properly designed antibody-chelate conjugate for radioimmunoconjugate could serve a therapeutic agent or imaging probe by introduced radioisotope. ^{90}Y-labeled Ibritumomab tiuxetan (Zevalin®) is a radioimmunotherapy pharmaceutical for recurrent and resistant forms of low-grade follicular B-cell non-Hodgkin's lymphoma. SPECT imaging with ^{111}In labeled Ibritumomab tiuxetan was performed to select the right patients for Zevalin treatment (*16*).

Because antibody molecules are very labile to heat, pH, and agents such as salt and detergents, forming antibody-chelator conjugates before introducing the radioisotope is a proper strategy for preparation and quality control of radiopharmaceuticals with antibody molecules. In particular, an appropriately structured antibody-chelator conjugate could be applicable for therapeutic or imaging purposes by introducing a metallic therapeutic or imaging radioisotope such as ^{90}Y-labeled Ibritumomab tiuxetan or ^{111}In-labeled Ibritumomab tiuxetan. ^{64}Cu with a half-life of 12.7 h is the most widely studied PET radioisotope. It can be produced via the ^{64}Ni(p,n)^{64}Cu reaction using a cyclotron in a carrier-free state (*17*). The optimal structure of the antibody-chelator conjugate for ^{64}Cu could be used for therapeutic beta-emitter ^{67}Cu (half-life of 2.58 d) as a pair of radioisotopes of ^{64}Cu (*18*). Because ^{64}Cu-radiolabeled complexes with improved stability have been reported with 1,4,7-triazacyclononane-1,4,7-triacetic acid (NOTA) derivatives (*19*), we introduced NOTA as a chelator for ^{64}Cu labeling into trastuzumab antibody to provide more favorable pharmacokinetic of ^{64}Cu-labeled trastuzumab than that of DOTA as a chelator. Moreover, we can predict the internal radiation absorbed dose of ^{67}Cu-labeled antibody using ^{64}Cu-labeled antibody (*20,21*), which is a powerful advantage for ^{64}Cu/^{67}Cu-labeled antibody development as a PET probe or therapeutic agent (Supplemental Fig. 1).

The purpose of this study was to develop ^{64}Cu-labeled trastuzumab using NOTA as a chelator with

improved pharmacokinetics for HER2 and to evaluate the pharmacokinetic characteristics and image-based absorbed dose of ^{64}Cu-NOTA-trastuzumab for human study.

Materials and Methods

Small animal PET/CT imaging

At 1, 2, and 6 h, and 1, 2, and 3 days after the intravenous injection of 7.4 MBq of ^{64}Cu-NOTA-trastuzumab per animal, mice were placed in a spread prone position under inhalation anesthesia (isoflurane, 2%) and imaged for 20 min with an Inveon dedicated small animal PET/CT scanner (Siemens Healthcare; n = 3). The counting rates in the reconstructed images were converted to activity concentrations (percentage injected dose [%ID] per gram of tissue). To define each organ and tumor in the mice, we acquired contrast CT data using ExiTron nano 12000 (Miltenyi Biotec, Auburn, CA, USA). Blocking studies (n = 2) were carried out to evaluate HER2 specificity of ^{64}Cu-NOTA-trastuzumab *in vivo*, where a group of two mice were each injected with 1 mg of non-labeled trastuzumab within 1 h before ^{64}Cu-NOTA-trastuzumab administration.

Analysis of time activity curve and residence time

Mouse images were acquired at six time points after the radiotracer administration. PET image data and CT image data were co-localized and the PET image data were segmented for each organ and tumor to calculate time activity curve and S-value. Individual mouse CT data were segmented by referral to the contrast CT image. Tumor and organs were segmented by mean-based region growing three-dimensional segmentation method. The time activity curve was expressed by %ID/g where the injected dose of radioactivity in target region (ID) divided by target region mass (g). Residence times were calculated via time activity curves of acquired region segmented PET data.

Results

Quantification of ^{64}Cu-NOTA-trastuzumab in HER2-positive breast tumor PET images

To evaluate the potential of ^{64}Cu-NOTA-trastuzumab as a PET imaging agent for HER2 expression, we performed PET imaging in ectopic BT-474 tumor models. BT-474 tumors were clearly visible on PET images after 24 h (Fig. 1). Quantitative data obtained from ROI analysis of the PET results in non-blocking group are shown in Fig. 2A. Liver uptake values for ^{64}Cu-NOTA-trastuzumab were 14.64 ± 2.23, 13.23 ± 1.34, and 9.50 ± 0.32 %ID/g at 24, 48, and 72 h, respectively (n = 3). Radioactivity in the blood was 19.23 ± 4.43, 15.00 ± 2.45, and 13.03 ± 3.71 %ID/g at 24, 48, and 72 h, respectively (n = 3). Importantly, tumor uptake of ^{64}Cu-NOTA-trastuzumab accumulated and was clearly visible at 24 h, peaked at 48 h, and remained prominent over time (24.82 ± 11.16, 29.24 ± 16.45, and 28.34 ± 15.89 %ID/g at 24, 48, and 72 h, respectively; n = 3).

Administering a blocking dose of trastuzumab 1 h prior to ^{64}Cu-NOTA-trastuzumab injection significantly reduced tumor uptake to 6.80 ± 0.77, 6.85 ± 1.73 and 6.70 ± 0.49 %ID/g at 24, 48, and 72 h, respectively (n = 2; Fig. 2B), which demonstrated that ^{64}Cu-NOTA-trastuzumab maintained the HER2 specificity of its parent antibody *in vivo*. Liver uptake of ^{64}Cu-NOTA-trastuzumab in the blocking group was similar to that in mice injected with ^{64}Cu-NOTA-trastuzumab alone: 17.72 ± 2.53, 15.67 ± 0.27 and 12.30 ± 1.66 %ID/g at 24, 48, and 72 h, respectively (n = 2).

Moreover, orthotopic BT-474 tumor uptake of ^{64}Cu-NOTA-trastuzumab accumulated and was clearly visible at 6 h, peaked at 51 h, and remained prominent over time (2.48 ± 1.69, 3.08 ± 2.47, 3.53 ± 2.99 and 2.92 ± 3.92 %ID/g at 6, 28, 51, and 122 h, respectively). An autoradiogram of the frozen section prepared from the removed HER2-positive tumor revealed great accumulation in the areas where HER2-positive cells were detected by IHC (Fig. 3).

Biodistribution of ^{64}Cu-NOTA-trastuzumab in HER2-positive breast tumor model and normal mice

Biodistribution data of ^{64}Cu-NOTA-trastuzumab in BT-474 HER2-positive tumor models was compared and is summarized in Fig. 4. The ^{64}Cu-NOTA-trastuzumab uptake of major organs and tissues in tumor bearing mice were similar in normal mice. The radioactivities in blood and spleen were high at 2 h, but gradually decreased over time. The uptake of ^{64}Cu-NOTA-trastuzumab in BT-474 HER2-positive tumors steadily increased and peaked at 48 h at 64.44 ± 31.11 %ID/g.

Pharmacokinetics of ^{64}Cu-NOTA-trastuzumab in nude mice with or without HER2 positive tumor

The blood radioactivity concentration-time profiles following single i.v. bolus injection of ^{64}Cu-NOTA-trastuzumab in nude mice with or without BT-474 tumor xenograft are shown in Fig. 5. In both groups of mice, blood radioactivity concentrations decreased bi-exponentially with time. The concentration-time profiles in tumor-bearing nude mice were similar to those in the nude mice without tumors. Table 1 summarizes the pharmacokinetic parameters obtained by non-compartmental analysis. The blood concentration extrapolated to time zero (C_0) was 46.8 ± 7.52 and 48.7 ± 4.64 %ID/mL; the terminal elimination half-life ($t_{1/2,\lambda z}$) was 135 ± 41.1 and 190 ± 40.2 h; the area under the blood concentration-time curve ($AUC_{0\text{-}72h}$) was 1354 ± 166 and 1480 ± 124 %ID·h/mL; the volume of distribution at terminal phase (V_z) was 4.74 ± 0.786 and 4.69 ± 0.461 mL; the systemic clearance (Cl) was 0.0254 ± 0.00538 and 0.0176 ± 0.00289 mL/h; and the mean retention time (MRT) was 31.0 ± 0.512 and 31.6 ± 0.390 h, respectively, after i.v. injection of ^{64}Cu-NOTA-trastuzumab in nude mice with and without tumors.

Residence time calculation

To clearly define each organ region, we acquired CT images using a contrast agent. As a result we clearly defined the ROI in PET image data. The segmented tumor and major organs are shown in Fig. 6A. Time activity curve was calculated at each time point (1, 2, and 6 h, and 1, 2, and 3 days) using the defined specific region in PET image (Fig. 6B). The highest mean residence time was in the tumor, followed by the kidney, heart, liver, lung, urinary bladder, spleen, and stomach; the lowest residence time region was the brain (Fig. 6C). The mean residence time in the tumors was 7.42 ± 3.3 MBq-h/MBq. The residence time in the heart was 3.33 ± 0.8 MBq-h/MBq. The residence time in the lung was 2.28 ± 0.7, and that in the liver was 2.66 ± 0.8 MBq-h/MBq. The residence time in the stomach was 1.31 ± 0.2, and that in the spleen was 2.19 ± 0.6 MBq-h/MBq.

Absorbed dose calculation

S-value was calculated with both ^{64}Cu and ^{67}Cu using Monte Carlo simulation with the CT images. As shown in Table 2, S-value was higher with the self- rather than cross-irradiation and highest in the HER2-positive tumors, followed by the spleen, brain, urinary bladder, heart, kidney, and liver. We calculated the absorbed dose of ^{64}Cu-NOTA-trastuzumab using an image-based approach. The absorbed dose of ^{64}Cu-NOTA-trastuzumab was 0.048 ± 0.012 for heart, 0.079 ± 0.004 for liver, 0.047 ± 0.010 for spleen, and 2.43 ± 1.09 mGy/MBq for tumor. According to a study by Tamura et al. (12), the absorbed dose of ^{64}Cu-DOTA-trastuzumab was 0.34 ± 0.046 for heart, 0.24 ± 0.117 for liver, and 0.14 ± 0.04 mGy/MBq for spleen (Fig. 7). Consequently, the absorbed dose of ^{64}Cu-NOTA-trastuzumab was lower than those of ^{64}Cu-DOTA-trastuzumab in the heart, liver and spleen. We also calculated the absorbed dose of ^{67}Cu-NOTA-trastuzumab using Monte Carlo simulation to develop ^{67}Cu-NOTA-trastuzumab as a therapeutic agent for HER2-positive breast cancer based on ^{64}Cu-NOTA-trastuzumab. Absorbed dose of ^{67}Cu-NOTA-trastuzumab and ^{67}Cu-DOTA-trastuzumab in liver were 0.042 mGy/MBq and 0.934 mGy/MBq calculated

using the biodistribution results published by Paudyal et al. (*22*), respectively. Therefore ^{67}Cu-NOTA-trastuzumab might be safer than ^{67}Cu-DOTA-trastuzumab because of the lower absorbed dose in major organs such as liver, heart, and spleen.

Discussion

Breast cancer is the most common malignancy. It is a heterogeneous disease that can be classified by microscopic appearance and molecular profiles that include the expression of estrogen receptor and overexpression of HER2 (*3*). Overexpression of HER2 portends a poor prognosis with an increased risk for disease progression and decreased overall survival (*23*).

The discovery of many novel molecular targets for anticancer treatment has led to the development of therapeutic antibodies. Overexpression of HER2 enables constitutive activation of growth factor signaling pathways and thereby serves as an oncogenic driver in breast cancer. Through both genetic and pharmacologic approaches it was determined that HER2 is both necessary and sufficient for tumor formation and maintenance in models of HER2-positive breast cancer (*24*). Targeting HER2 with mAb, such as trastuzumab and pertuzumab, is a well-established therapeutic strategy for HER2-positive breast cancer in neoadjuvant (*25*), adjuvant (*26,27*), and metastatic settings (*28,29*). Especially trastuzumab (Herceptin®), a humanized recombinant mAb against HER2, is widely used as a standard treatment for HER2-expressing breast cancer. Recently, a need has been recognized for the repetitive visualization of HER2 expression due to development success of trastuzumab-emtansine as an antibody-drug conjugate to minimize the toxicity against major organs and enhance the therapeutic efficacy. Detection of HER2-positive metastatic tumor using radio-labeled HER2 antibodies would be valuable to provide safety, treatment economy, and other therapeutic options to HER2-negative tumor-bearing patients. Conversely, Ulaner et al. reported that ^{89}Zr-labeled trastuzumab PET/CT could be applied to detect unsuspected HER2-positive metastases in patients with HER2-negative primary breast cancer as a proof-of-concept clinical study (*29*). Thus, it is important to evaluate HER2 expression in metastatic as well as primary tumors to determine whether anti-HER2 therapy is indicated.

Although HER2 expression is routinely determined using histological analysis (*30*), technical problems

can arise when lesions cannot be easily accessed by core-needle biopsy, and the analysis lacks specificity and sensitivity (*31*). In addition, HER2 expression can be variable during the course of the disease and even across tumor lesions within the same patient. To overcome these problems, novel techniques, such as PET and SPECT have been studied for evaluating HER2 expression. Molecular imaging using radio-labeled antibodies can provide real-time information and noninvasively assess the presence of specific targets throughout the body (*32*). PET imaging depends on the delivery of a targeting ligand containing a positron emitting radionuclide to a tissue or organ of interest. ^{64}Cu ($t_{1/2}$ = 12.7 h) is an attractive radionuclide for PET imaging that can be used for both diagnostic imaging and radionuclide therapy due to its dual decay characteristics (*33*). PET images acquired by ^{64}Cu-labeled trastuzumab could potentially achieve good contrast with high resolution and low radiation exposure because of the shorter half-life of the radioisotope (*12*). However, the application of ^{64}Cu as a radioisotope for antibody molecules has been hindered by the lack of an optimal chelator to form a stable conjugate complex *in vivo*. The high uptake and retention of copper-containing compounds in the blood and liver are well known (*34,35*). Therefore, an optimal chelator for copper metal ion for a more stable conjugate is required for *in vivo* studies using ^{64}Cu. 1,4,7-Triazacyclononane-1,4,7-triacetic acid (NOTA) is an intensively investigated macrocyclic, multi-dentate chelator used for complexation of a broad variety of bi- and trivalent metal ions (*36-38*). Bifunctional NOTA forms an exceedingly stable complex with Ga^{3+} ions, and PET agents can feature its use. NOTA conjugates labeled with ^{67}Ga, ^{68}Ga, ^{64}Cu, ^{67}Cu, and ^{111}In are suitable for diagnostic and therapeutic approaches (*39,40*). According to Paudyal's report (*22*), the uptake of ^{64}Cu-DOTA-trastuzumab in liver was 26.9 ± 7.4 %ID/g at 24h. On the contrary, the uptake of ^{64}Cu-NOTA-trastuzumab was 5.44 ± 1.84 %ID/g in liver at 24 h (Fig. 4). This result suggests that release of ^{64}Cu from ^{64}Cu-NOTA-trastuzumab is less than that from ^{64}Cu-DOTA-trastuzumab, and therefore that ^{64}Cu-NOTA-trastuzumab is more stable than ^{64}Cu -DOTA-trastuzumab.

According to the pharmacokinetic results of ^{64}Cu-NOTA-trastuzumab in HER2-positive tumor and

non-tumor bearing nude mice, the systemic clearance and terminal half-life were significantly different from each other ($p<0.05$; Fig. 5), whereas other parameters were quite similar to each other. The systemic clearance in nude mice with HER2-positive tumor was higher than that in nude mice without tumors. This result suggests that the elimination rate of ^{64}Cu-NOTA-trastuzumab in nude mice with HER2-positive tumor is faster than that in nude mice without tumor and this might be because ^{64}Cu-NOTA-trastuzumab is targeted, trapped to HER2-positive tumor, and removed from mouse circulation.

The image-based methods basically include Monte Carlo simulation and entail manually drawing ROI to calculate the individual specific dosimetry based on the patient's anatomical image. Monte Carlo simulation can be used for acquiring S-value of different radionuclide. If the same pharmacokinetic or pharmacodynamics characteristics between diagnostic radiopharmaceutical such as emitting gamma ray and therapeutic radiopharmaceuticals such as emitting alpha or beta particles, it could be possible to calculate the subject-specific internal dosimetry using diagnostic radiopharmaceutical (*41*). In order to develop ^{67}Cu-NOTA-trastuzumab as therapeutic agent based on ^{64}Cu-NOTA-trastuzumab, we calculated the absorbed dose of ^{67}Cu-NOTA-trastuzumab in this study using Monte Carlo simulation. Consequently, lower absorbed dose of ^{67}Cu-NOTA-trastuzumab in major organs exhibited safer than ^{67}Cu-DOTA-trastuzumab. Therefore, NOTA-conjugated trastuzumab might be applicable for therapeutic as well as PET diagnostic for HER2 positive breast cancer.

Conclusion

Trastuzumab as an HER2-targeting antibody can be efficiently radiolabeled with ^{64}Cu using NOTA as a chelator with high labeling yield and excellent stability. The calculated absorbed dose of ^{64}Cu-NOTA-trastuzumab was lower than those of ^{64}Cu-DOTA-trastuzumab in heart, liver and spleen due to short residence time. Furthermore, ^{64}Cu-NOTA-trastuzumab was efficiently targeted to the HER2-expressing tumor *in vivo* and *in vitro*. Therefore, ^{64}Cu-NOTA-trastuzumab could be applicable in human studies to select patients with the right timing for HER2 therapy, while monitoring the treatment response after HER2-targeted therapy.

Acknowledgment

This work was supported by the National Research Foundation of Korea (NRF) grant funded by the Ministry of Science & ICT (NRF-2012M2A2A7013480, NRF-2015R1C1A1A02036885 and NRF-2017M2A2A02070985).

Research involving animals

All animal experiments were carried out under a protocol approved by the KIRAMS Institutional Animal Care and Use Committee (kirams2016-0097).

References

1. Okines AF, Cunningham D. Trastuzumab in gastric cancer. *Eur J Cancer*. 2010;46:1949-1959.

2. Schrama D, Reisfeld RA, Becker JC. Antibody targeted drugs as cancer therapeutics. *Nat Rev Drug Discov*. 2006;5:147-159.

3. Slamon DJ, Clark GM, Wong SG, et al. Human breast cancer: correlation of relapse and survival with amplification of the HER-2/neu oncogene. *Science*. 1987;235:177-182.

4. Loibl S, Gianni L. HER2-positive breast cancer. *Lancet*. 2017;389:2415-2429.

5. Jiang H, Rugo HS. Human epidermal growth factor receptor 2 positive (HER2+) metastatic breast cancer: how the latest results are improving therapeutic options. *Ther Adv Med Oncol*. 2015;7:321-339.

6. Gebhart G, Flamen P, De Vries EG, et al. Imaging diagnostic and therapeutic targets: human epidermal growth factor receptor 2. *J Nucl Med*. 2016;57:81S-88S.

7. Niu G, Li Z, Cao Q, et al. Monitoring therapeutic response of human ovarian cancer to 17-DMAG by noninvasive PET imaging with ^{64}Cu-DOTA-trastuzumab. *Eur J Nucl Med Mol Imaging*. 2009; 36:1510-1519.

8. Orlova A, Wållberg H, Stone-Elander S, et al. On the selection of a tracer for PET imaging of HER2-expressing tumors: direct comparison of a ^{124}I-labeled affibody molecule and trastuzumab in a murine xenograft model. *J Nucl Med*. 2009;50:417–425.

9. Perik PJ, Lub-De Hooge MN, Gietema JA, et al. Indium-111-labeled trastuzumab scintigraphy

in patients with human epidermal growth factor receptor 2-positive metastatic breast cancer. *J Clin Oncol*. 2006;24:2276-2282.

10. Dijkers EC, Kosterink JG, Rademaker AP, et al. Development and characterization of clinical-grade ^{89}Zr-trastuzumab for HER2/neu immunoPET imaging. *J Nucl Med*. 2009;50:974–981.

11. Kurihara H, Hamada A, Yoshida M, et al. ^{64}Cu-DOTA-trastuzumab PET imaging and HER2 specificity of brain metastases in HER2-positive breast cancer patients. *EJNMMI Research*. 2015;5:8.

12. Tamura K, Kurihara H, Yonemori K, et al. ^{64}Cu-DOTA-trastuzumab PET imaging in patients with HER2-positive breast cancer. *J Nucl Med*. 2013;54:1869-1875.

13. Mortimer JE, Bading JR, Colcher DM, et al. Functional Imaging of Human Epidermal Growth Factor Receptor 2-Positive Metastatic Breast Cancer Using ^{64}Cu-DOTA-Trastuzumab PET. *J Nucl Med*. 2014;55(1):23-29.

14. Mortimer JE, Bading JR, Park JM, et al. Tumor Uptake of ^{64}Cu-DOTA-Trastuzumab in Patients with Metastatic Breast Cancer. *J Nucl Med*. 2018;59(1):38-43.

15. Kristensen L, Nielsen C, Nedergaard M, et al. ^{64}Cu-DOTA-trastuzumab imaging in a HER2-positive intracranial patient-derived xenograft (PDX) model of breast cancer metastasis. *J Nucl Med*. 2016;57(supplement 2):1338.

16. Rizzieri D. Zevalin®(ibritumomab tiuxetan): After more than a decade of treatment

experience, what have we learned? *Crit Rev Oncol Hematol*. 2016;105:5-17.

17. Kim KI, Jang SJ, Park JH, et al. Detection of increased ^{64}Cu uptake by human copper transporter 1 gene overexpression using PET with $^{64}CuCl_2$ in human breast cancer xenograft model. *J Nucl Med*. 2014;55:1692-1698.

18. Kraeber-Bodéré F, Rousseau C, Bodet-Milin C, et al. Tumor immunotargeting using innovative radionuclides. *Int J Mol Sci*. 2015;16:3932-3954.

19. Prasanphanich AF, Nanda PK, Rold TL, et al. [^{64}Cu-NOTA-8-Aoc-BBN(7-14)NH_2] targeting vector for positron-emission tomography imaging of gastrin releasing peptide receptor-expressing tissues. *Proc Natl Acad Sci U S A*. 2007;104:12462–12467.

20. Bouchet LG, Bolch WE, Blanco HP, et al. MIRD Pamphlet No. 19: Absorbed fractions and radionuclide S values for six age-dependent multiregion models of the kidney. *J Nucl Med*. 2003;44:1113-1147.

21. Park YS, Lee YJ, Kim W, et al. Image-based Absorbed Dosimetry of Radioisotope. *Prog Med Phys*. 2016;27:86-91.

22. Paudyal P, Paudyal B, Hanaoka H, et al. Imaging and biodistribution of Her2/neu expression in non-small cell lung cancer xenografts with ^{64}Cu-labeled trastuzumab PET. *Cancer Sci*. 2010;101:1045-1050.

23. Sjögren S, Inganäs M, Lindgren A, et al. Prognostic and predictive value of c-erbB-2 overexpression in primary breast cancer, alone and in combination with other prognostic

markers. *J Clin Oncol*. 1998;16:462-469.

24. Buzdar AU, Ibrahim NK, Francis D, et al. Significantly higher pathologic complete remission rate after neoadjuvant therapy with trastuzumab, paclitaxel, and epirubicin chemotherapy: results of a randomized trial in human epidermal growth factor receptor 2–positive operable breast cancer. *J Clin Oncol*. 2005;23:3676-3685.

25. Piccart-Gebhart MJ, Procter M, Leyland-Jones B, et al. Trastuzumab after adjuvant chemotherapy in HER2-positive breast cancer. *N Engl J Med*. 2005;353:1659-1672.

26. Romond EH, Perez EA, Bryant J, et al. Trastuzumab plus adjuvant chemotherapy for operable HER2-positive breast cancer. *N Engl J Med*. 2005;353:1673-1684.

27. Slamon DJ, Leyland-Jones B, Shak S, et al. Use of chemotherapy plus a monoclonal antibody against HER2 for metastatic breast cancer that overexpresses HER2. *N Engl J Med*. 2001;344:783-792.

28. Tripathy D, Slamon DJ, Cobleigh M, et al. Safety of treatment of metastatic breast cancer with trastuzumab beyond disease progression. *J Clin Oncol*. 2004;22:1063-1070.

29. Ulaner GA, Hyman DM, Lyashchenko SK, et al. ^{89}Zr-trastuzumab PET/CT for Detection of Human Epidermal Growth Factor Receptor 2–positive Metastases in Patients With Human Epidermal Growth Factor Receptor 2–negative Primary Breast Cancer. *Clin Nucl Med*. 2017;42:912-917.

30. Sauter G, Lee J, Bartlett JM, et al. Guidelines for human epidermal growth factor receptor 2

testing: biologic and methodologic considerations. *J Clin Oncol*. 2009;27:1323-1333.

31. Lebeau A, Turzynski A, Braun S, et al. Reliability of human epidermal growth factor receptor 2 immunohistochemistry in breast core needle biopsies. *J Clin Oncol*. 2010;28:3264-3270.

32. Song IH, Lee TS, Park YS, et al. Immuno-PET imaging and radioimmunotherapy of ^{64}Cu-/^{177}Lu-labeled anti-EGFR antibody in esophageal squamous cell carcinoma model. *J Nucl Med*. 2016;57:1105-1111.

33. Wadas T, Wong E, Weisman G, et al. Copper chelation chemistry and its role in copper radiopharmaceuticals. *Curr Pharm Des*. 2007;13:3-16.

34. Bearn A, Kunkel HG. Localization of ^{64}Cu in serum fractions following oral administration: an alteration in Wilson's disease. *Proc Soc Exp Biol Med*. 1954;85:44-48.

35. Owen CA, Hazelrig JB. Metabolism of ^{64}Cu-labeled copper by the isolated rat liver. *Am J Physiol*. 1966;210:1059-1064.

36. Wieghardt K, Bossek U, Chaudhuri P, et al. 1, 4, 7-Triazacyclononane-N, N', N''-triacetate (TCTA), a new hexadentate ligand for divalent and trivalent metal ions. Crystal structures of [CrIII (TCTA)],[FeIII (TCTA)], and Na [CuII (TCTA)]·2NaBr·8H_2O. *Inorg Chem*. 1982;21:4308-4314.

37. Cacheris W, Nickle S, Sherry A. Thermodynamic study of lanthanide complexes of 1, 4, 7-triazacyclononane-N, N', N''-triacetic acid and 1, 4, 7, 10-tetraazacyclododecane-N, N', N'', N'''-tetraacetic acid. *Inorg Chem*. 1987;26:958-960.

38. Boeyens JC, van der Merwe MJ. The Nonexistent Crystals of Macrocyclic Nickel (III). Structure of the Cobalt (III) Complex of 1, 4, 7-Triazacyclononane-N, N ‘, N ‘‘-triacetate. *Inorg Chem*. 1997;36:3779-3780.

39. Roosenburg S, Laverman P, Joosten L, et al. PET and SPECT imaging of a radiolabeled minigastrin analogue conjugated with DOTA, NOTA, and NODAGA and labeled with ^{64}Cu, ^{68}Ga, and ^{111}In. *Mol Pharm*. 2014;11:3930-3937.

40. Guleria M, Das T, Amirdhanayagam J, et al. Comparative evaluation of using NOTA and DOTA derivatives as bifunctional chelating agents in the preparation of ^{68}Ga-labeled Porphyrin: Impact on pharmacokinetics and tumor uptake in a mouse model. *Cancer Biother Radiopharm*. 2018;33:8-16.

41. Huang S-y, Bolch WE, Lee C, et al. Patient-specific dosimetry using pretherapy [^{124}I] m-iodobenzylguanidine ([^{124}I] mIBG) dynamic PET/CT imaging before [^{131}I] mIBG targeted radionuclide therapy for neuroblastoma. *Mol Imaging Biol*. 2015;17:284-294.

Figure 1

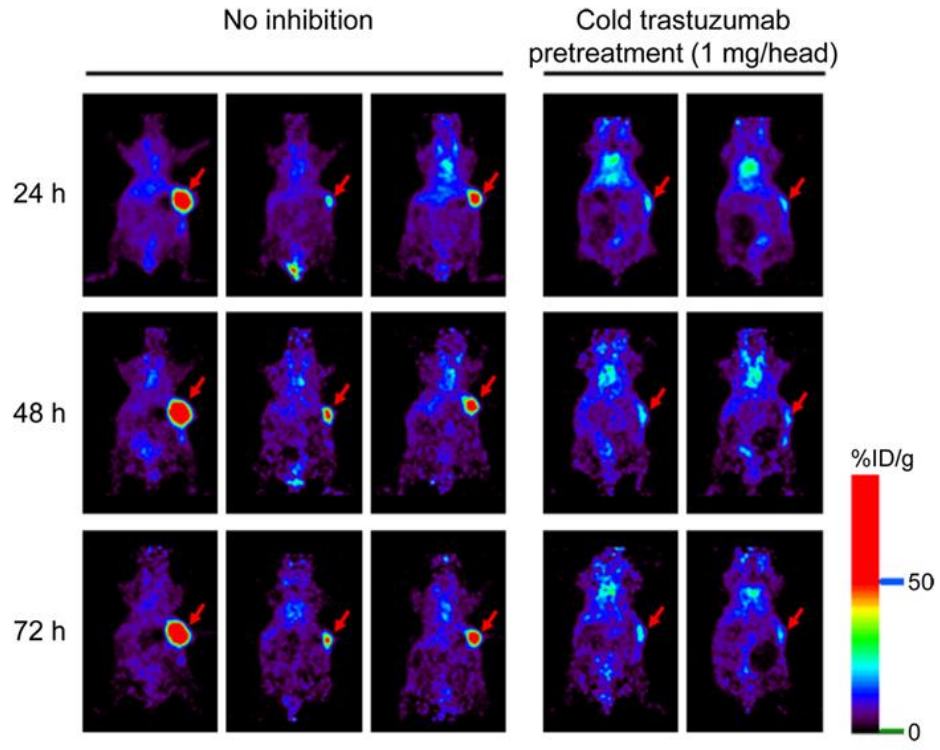

Figure 1. ^{64}Cu-NOTA-trastuzumab PET images in an HER2-positive tumor model. The right two columns display PET images after cold trastuzumab pretreatment (n=2), and the left three show non-blocking images (n=3). Red arrows indicate BT-474 tumors.

Figure 2

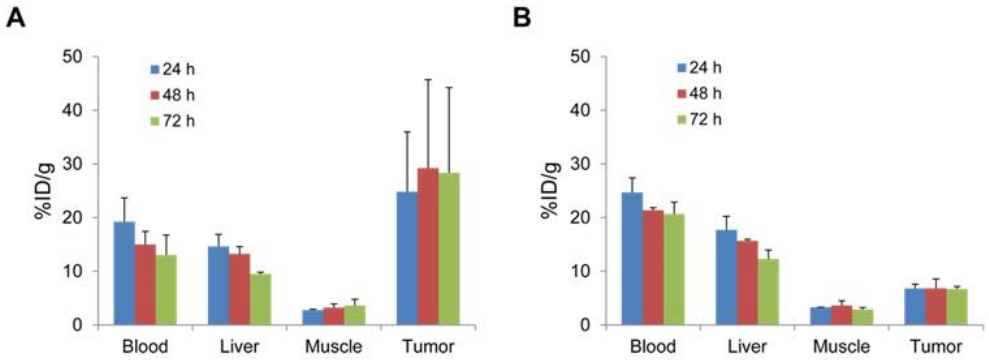

Figure 2. ^{64}Cu-NOTA-trastuzumab PET image quantification of non-blocking group (A) and cold trastuzumab pretreated group (B) in HER2-positive tumor model. ^{64}Cu-NOTA-trastuzumab specificity was suggested by blocking experiments with an excess of unlabeled trastuzumab.

Figure 3

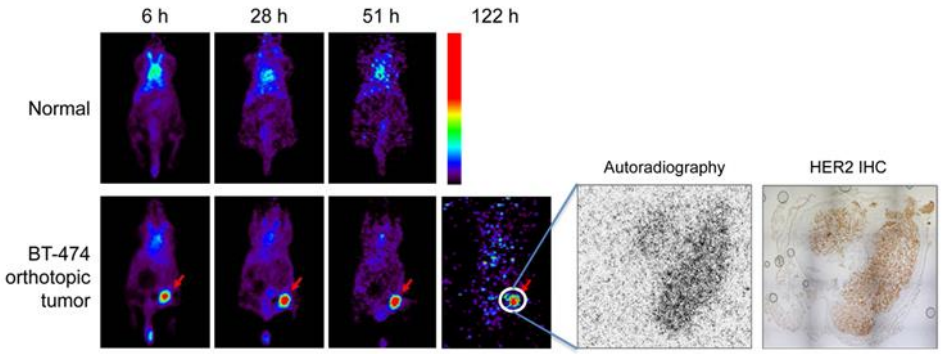

Figure 3. ^{64}Cu-NOTA-trastuzumab PET and immunohistochemistry in an orthotopic HER2-positive BT-474 breast tumor model. Tumor uptake of ^{64}Cu-NOTA-trastuzumab was clearly visible at 6 h, and peaked at 51 h, and an autoradiogram of the frozen section prepared from the removed tumor revealed great accumulation in the area where HER2-positive cells were detected by IHC.

Figure 4

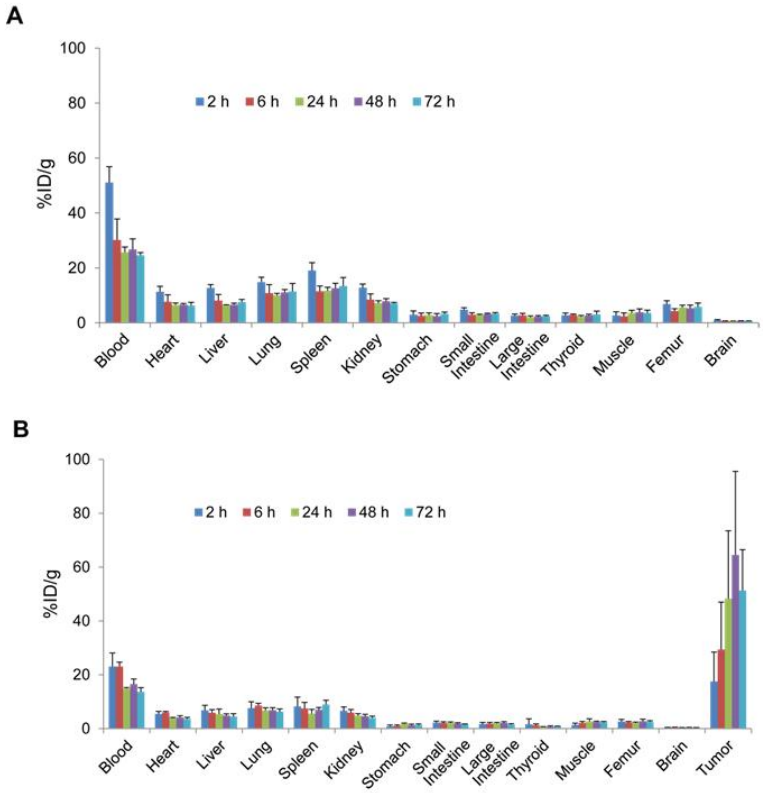

Figure 4. Biodistribution of ^{64}Cu-NOTA-trastuzumab in normal mice (A) and HER2-positive tumor bearing mice (B). At 2, 6, 24, 48, and 72 h after injection of ^{64}Cu-NOTA-trastuzumab, both mice were euthanized, and radioactivity in organs was measured (n = 4). Radioactivity in tissues is expressed as %ID/g.

Figure 5

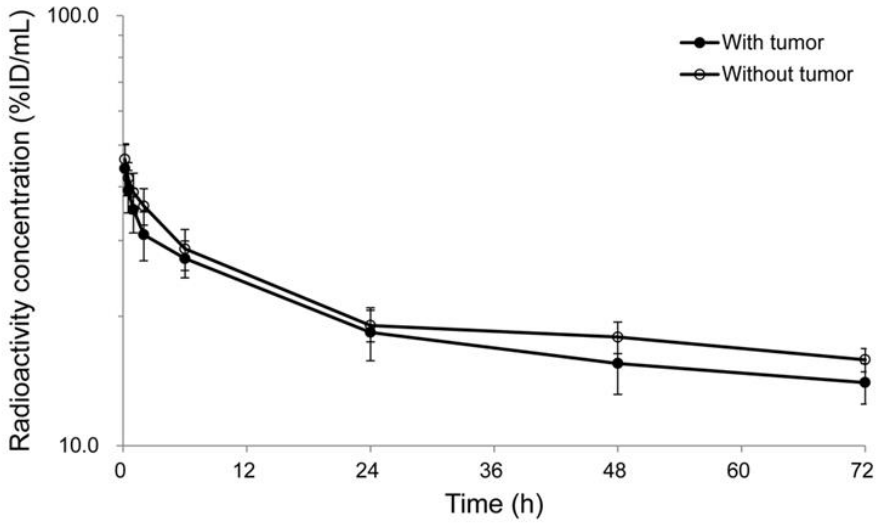

Figure 5. Average blood radioactivity concentration vs. time curve obtained after i.v. injection of ^{64}Cu-NOTA-Trastuzumab in nude mice with or without BT-474 tumor xenograft (dose 100 μg/150 -180 μCi/head, n = 6). Values are represented as mean %ID/mL ± SD. %ID/mL; the percent injected dose per milliliter of blood.

Figure 6

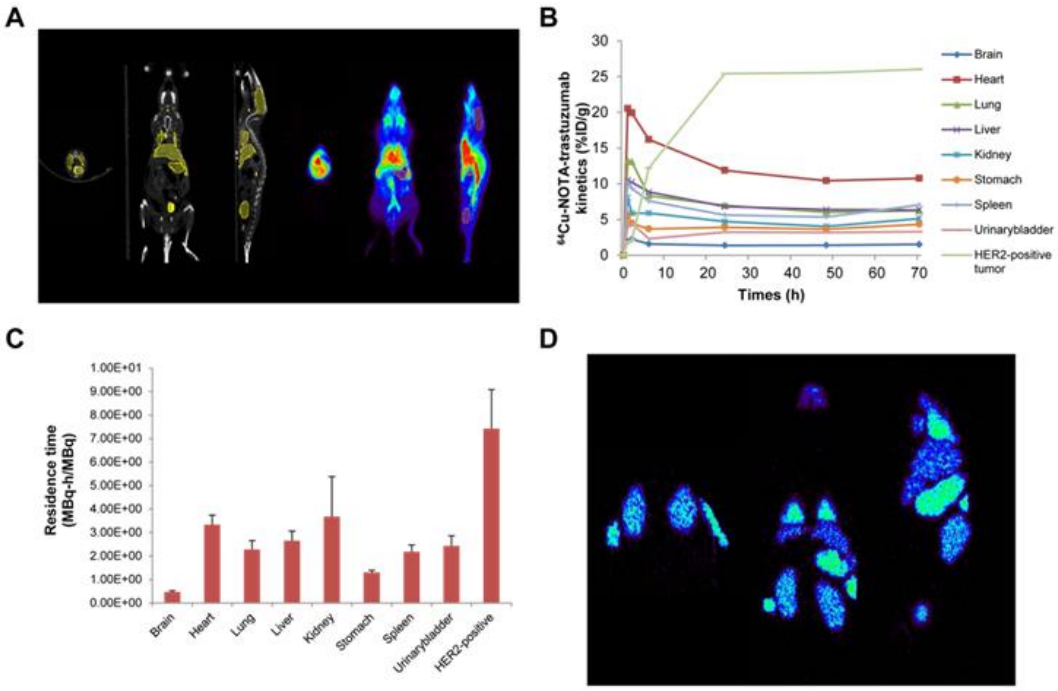

Figure 6. Acquired PET/CT image data and analysis. (A) Acquired CT and PET. (B) Time activity curve evaluated by segmented PET image data at six time points. (C) Calculated residence time in each organ and tumor. (D) Generated energy map from Monte Carlo simulation.

Figure 7

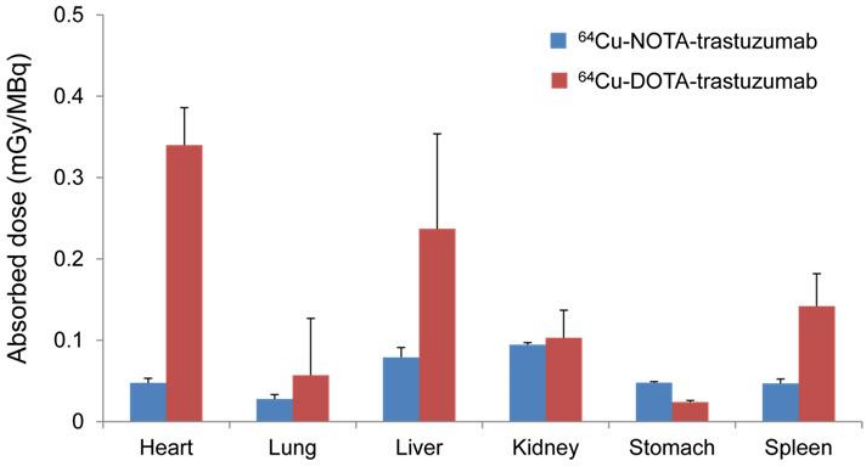

Figure 7. Comparison of the absorbed dose between ^{64}Cu-NOTA-trastuzumab and ^{64}Cu-DOTA-trastuzumab (*12*). ^{64}Cu-DOTA-trastuzumab exhibited higher absorbed dose than ^{64}Cu-NOTA-trastuzumab in the heart, liver and spleen.

Table 1

Table 1. Average pharmacokinetic parameters of radioactivity in blood obtained after i.v. injection of ^{64}Cu-NOTA-Trastuzumab in nude mice with and without BT-474 tumor xenograft (dose 100 μg/150~180 μCi/head)

Parameter	With tumor	Without tumor	P value
C_0 (%ID/mL)	46.8 ± 7.52	48.7 ± 4.64	0.605
$t_{1/2,\lambda z}$ (h)	135 ± 41.1	190 ± 40.2	0.041
$AUC_{0\sim72h}$ (%ID*h/mL)	1354 ± 166	1480 ± 124	0.167
V_z (mL)	4.74 ± 0.786	4.69 ± 0.461	0.892
Cl (mL/h)	0.0254 ± 0.00538	0.0176 ± 0.00289	0.011
MRT_{last} (h)	31.0 ± 0.512	31.6 ± 0.390	0.051

Values are represented as mean ± SD.

Table 2

Table 2. Calculated S-value of ^{64}Cu (A) and ^{67}Cu (B) using Monte Carlo simulation with CT image.

A. ^{64}Cu S-value

S-values	Brain	Heart	Lung	Liver	Kidney	Stomach	Spleen	Bladder	Tumor
Brain	1.87E-01	3.39E-05	2.34E-05	9.14E-06	4.02E-06	8.93E-06	4.71E-06	1.38E-06	4.00E-06
Heart	2.41E-05	1.05E-01	1.13E-03	1.97E-04	1.64E-05	4.17E-05	2.29E-05	4.30E-06	1.08E-05
Lung	2.23E-05	1.07E-03	1.32E-01	5.70E-04	3.23E-05	5.28E-05	2.86E-05	7.40E-06	1.86E-05
Liver	1.26E-05	2.08E-04	5.90E-04	2.12E-02	4.49E-05	5.56E-04	3.33E-04	1.23E-05	2.89E-05
Kidney	4.51E-06	2.16E-05	2.80E-05	4.06E-05	6.77E-02	1.08E-04	1.63E-04	2.55E-05	3.06E-04
Stomach	4.95E-06	3.97E-05	4.56E-05	5.67E-04	9.71E-05	6.92E-02	8.32E-04	2.02E-05	2.47E-05
Spleen	4.56E-06	1.74E-05	2.51E-05	3.30E-04	1.43E-04	8.22E-04	2.43E-01	2.24E-05	2.06E-05
Bladder	1.78E-06	6.84E-06	6.93E-06	1.07E-05	2.58E-05	2.26E-05	1.89E-05	1.13E-01	1.85E-05
Tumor	9.09E-06	2.65E-05	3.20E-05	5.90E-05	4.59E-04	4.74E-05	3.11E-05	4.61E-05	3.28E-01

B. ^{67}Cu S-value

S-values	Brain	Heart	Lung	Liver	Kidney	Stomach	Spleen	Bladder	Tumor
Brain	8.54E-02	1.30E-05	1.18E-05	6.75E-06	5.01E-06	4.97E-06	2.61E-06	1.31E-06	4.41E-06
Heart	1.23E-05	1.38E-01	4.79E-04	1.49E-04	1.19E-05	2.43E-05	9.16E-06	4.70E-06	1.21E-05
Lung	1.22E-05	5.17E-04	1.79E-01	5.47E-04	1.56E-05	2.46E-05	1.66E-05	4.74E-06	1.81E-05
Liver	8.11E-06	1.45E-04	5.02E-04	2.76E-02	2.43E-05	4.04E-04	2.13E-04	6.01E-06	2.57E-05
Kidney	4.46E-06	1.31E-05	1.45E-05	2.67E-05	8.33E-02	5.66E-05	1.02E-04	1.83E-05	2.81E-04
Stomach	5.35E-06	2.22E-05	2.42E-05	4.11E-04	5.88E-05	8.54E-02	3.14E-04	1.07E-05	2.35E-05
Spleen	4.15E-06	1.31E-05	1.38E-05	2.09E-04	1.00E-04	3.23E-04	3.07E-01	1.30E-05	1.69E-05
Bladder	1.80E-06	5.20E-06	3.45E-06	6.35E-06	1.74E-05	1.11E-05	1.35E-05	1.30E-01	1.70E-05
Tumor	3.03E-06	9.70E-06	1.04E-05	1.57E-05	1.80E-04	1.59E-05	1.17E-05	1.33E-05	4.01E-01